



HAL
open science

Orientation control of Platinum electrode grown on silicon using [Ca₂Nb₃O₁₀]- nanosheets as seed layer.

J J Manguèle, F. Baudouin, C. Cibert, B. Domenges, V. Demange, Maryline Guilloux-Viry, A. Fouchet, G. Poullain

► **To cite this version:**

J J Manguèle, F. Baudouin, C. Cibert, B. Domenges, V. Demange, et al.. Orientation control of Platinum electrode grown on silicon using [Ca₂Nb₃O₁₀]- nanosheets as seed layer.. Thin Solid Films, 2023, 765, pp.139640. 10.1016/j.tsf.2022.139640 . hal-03932189

HAL Id: hal-03932189

<https://hal.science/hal-03932189v1>

Submitted on 15 Feb 2023

HAL is a multi-disciplinary open access archive for the deposit and dissemination of scientific research documents, whether they are published or not. The documents may come from teaching and research institutions in France or abroad, or from public or private research centers.

L'archive ouverte pluridisciplinaire **HAL**, est destinée au dépôt et à la diffusion de documents scientifiques de niveau recherche, publiés ou non, émanant des établissements d'enseignement et de recherche français ou étrangers, des laboratoires publics ou privés.



Distributed under a Creative Commons Attribution - NonCommercial 4.0 International License

Highlights for Editor

- Control of Pt orientation using $[\text{Ca}_2\text{Nb}_3\text{O}_{10}]^-$ nanosheets and deposition conditions
- Deposition of textured (111) Pt films on Si under standard conditions
- Deposition of textured (200) Pt films on Si using adaptive conditions

Orientation control of Platinum electrode grown on silicon using $[\text{Ca}_2\text{Nb}_3\text{O}_{10}]^-$ nanosheets as seed layer.

J.J. Manguele^a, F. Baudouin^b, C. Cibert^{a*}, B. Domengès^a, V. Demange^b, M. Guilloux-Viry^b, A. Fouchet^a, G. Poullain^a

a. Normandie Univ, ENSICAEN, UNICAEN, CNRS, CRISMAT, 6, boulevard du Maréchal Juin, F-14050 Caen, France.

b. Univ Rennes, CNRS, ISCR – UMR 6226, ScanMAT - UMS 2001, 263, avenue du Général Leclerc, F-35042 Rennes, France.

* Corresponding author: e-mail : christophe.ciberti@ensicaen.fr

Orcid ID: 0000-0002-5601-348X

Abstract

Platinum (Pt) is a noble metal with low resistivity and resilience to oxidation, which is largely used in microelectronic devices. In order to facilitate the integration of Pt thin films on silicon substrate, we are showing the ability to control their orientation by using $[\text{Ca}_2\text{Nb}_3\text{O}_{10}]^-$ nanosheets (CNOns) as seed layer. Pt thin films were sputtered on silicon coated by CNOns (CNOns/SiO₂/Si), and on TiO₂/SiO₂/Si substrates for comparison, at temperatures ranging from room temperature up to 625°C. Under pure argon, highly (111) textured Pt thin films were obtained on both substrates, regardless of the deposition temperature. However, by using an oxygen/argon mixture, highly (200) textured films could be obtained, only on CNOns/SiO₂/Si substrate, when the substrate temperature is above 550°C. X-ray diffraction, scanning electron microscopy, and atomic force microscopy were used to characterize the crystalline quality, thickness, surface morphology and roughness of the Pt thin films. Their resistivity was measured at room temperature by the four-point probes method.

Keywords

Platinum thin film orientation, nanosheets, electrode, low temperature, silicon substrate.

Journal Pre-proof

1. Introduction

The employment of oxide perovskite thin films such as $\text{Pb}(\text{Zr},\text{Ti})\text{O}_3$ (PZT), and BaTiO_3 in microelectronic technologies requires the use of silicon substrates and electrodes. Platinum (Pt) is the most commonly used material as bottom electrode in various microelectronic devices due to its low resistivity, high stability under oxygen environment at high temperature, and high work function leading to small leakage current. Furthermore, the Pt lattice parameter of 0.393 nm shows good lattice matching with a number of perovskite materials, such as $(\text{Ba},\text{Sr})\text{TiO}_3$ (~ 0.39 nm), BiFeO_3 (~ 0.39 nm), PZT (~ 0.40 nm), LaNiO_3 (LNO ~ 0.38 nm). It is well known that the physical properties of these oxide materials are sensitive to many parameters: the orientation of the films, the orientation and the crystalline quality of bottom electrode, and the quality of the interface between the oxide film and the bottom electrode. For instance, some authors have shown that epitaxial PZT thin films with a strong (100) orientation, grown by radio-frequency (rf) magnetron sputtering on epitaxial (200) Pt thin film pre-deposited on MgO single crystal, gave high remnant polarization [1,2]. Cui *et al.*[3] have also shown that (001)Pt/(200)BaTiO₃/(001)Pt epitaxial trilayers grown on (100)MgO substrate leads to a good interface between BaTiO₃ and the Pt bottom electrode. Nevertheless, for industrial electronic applications, with a few exceptions, the use of single crystal substrates is not a solution, because of their cost and their limited size compared to silicon wafers.

Since oxide films with *c*-axis epitaxial growth are advantageous in various applications, different authors utilized oxide buffer layers such as PbTiO_3 [4], PbO [5], TiO_2 [6] to optimize the *c*-axis orientation of oxide films on (111) Pt electrode. The risk with the use of a buffer layer between the bottom electrode and the functional films is to create a so-called electrical dead layer between them, due to interdiffusion or residual lattice mismatch that may take place. The existence of such dead layer and its consequences on the electrical properties of ferroelectric capacitors has been the subject of numerous studies since the 1990s [7–15]. This nonferroelectric layers, exhibiting a low dielectric constant, can have an appreciable effect upon the electrical properties of PZT thin films leading to a decrease of the dielectric constant when film thickness is reduced and a marked tilt of hysteresis loops, resulting in a large drop of both remanent and maximum polarizations [7–9]. Different mechanisms have been proposed to explain their origin including formation of Schottky depletion layers at interfaces [10–12], formation of a thin passive layer arising from damages

during film deposition [13], development of a nonferroelectric layer at the initial stage of PZT growth [8], or charge injection through an insulating layer [14]. It has also been shown that the electrical disturbances generated by the dead layer can be modeled and that the electrical characteristics of the ferroelectric film alone are masked by the existence of this passive layer [15]. Recent works have shown that the use of nanosheets deposited on platinized silicon [16], or even on platinized stainless steel [17], allows to obtain PZT films of very good quality (polarization of about 30-35 $\mu\text{C}/\text{cm}^2$) with very little fatigue after 10^{10} cycles. In these works, the nanosheets do not seem to have introduced a significant passive layer, since the electrical properties are very good. This is probably due to their very thin thickness of about a few nanometers. However, trying to grow (200)-oriented Pt electrode that allows epitaxial growth of oxide films directly on the bottom electrode without any buffer layer still remains a way to prevent such dead layer and to obtain a better quality of oxide/electrode interface [3].

Another possibility to obtain c-axis oriented oxide films with epitaxial growth and good interface quality is the use of oxide electrodes on silicon like LNO [18], SrRuO₃ [19], etc. In the case of LNO, it is possible to deposit films by RF sputtering at low temperature and still obtain well-crystallized films as early as 150°C [20] or 200 to 300°C [21]. However, the composition of these films is strongly dependent on the deposition temperature, which limits the adaptability of the process, and the resistivities obtained are an order of magnitude higher than those of Pt (400 $\mu\Omega\cdot\text{cm}$ for LNO against 10 to 20 $\mu\Omega\cdot\text{cm}$ for Pt). The residual stress of these films is also difficult to control as shown in the study of Zhao *et al* [22]. In the case of SrRuO₃, high temperatures above 600°C are still required to obtain well crystallized films. However, this kind of oxide electrodes have shown their interest to obtain functional films like ferroelectric PZT films with excellent properties. But it has also been shown that excellent ferroelectric properties, with for example polarization higher than 45 $\mu\text{C}/\text{cm}^2$ can be achieved on platinum electrodes [2,8,23]. Finally, the sputtering of oxide films with a chemical composition including two cations will generally remain more complicated than depositing a simple metal electrode like Pt.

When grown under standard conditions on SiO₂/Si substrates with a TiO₂ buffer layer, Pt thin films are only (111)-oriented and well-crystallized films on TiO₂/SiO₂/Si substrates are obtained at temperatures above 600°C [24–28]. This unique orientation is due to lowest surface energy associated with (111) planes [29]. Buffer layers like Ta, Zr or ZrO₂ [30,31]

have also been tried, but TiO_2 is still widely used for adhesion of the Pt bottom electrode. For all these buffer layers, only (111)-oriented Pt was obtained on silicon substrates. Some efforts have been done to obtain a preferential (200) orientation for Pt films without single crystal by using very high temperatures ($> 750^\circ\text{C}$) and a deposition gas containing a mixture of argon and oxygen [32,33]. Moreover, Park *et al.* [34] used direct current magnetron sputtering with Ar/O_2 gas mixture to deposit Pt thin films on SiO_2/Si without buffer layer, and obtained fully oriented (200) Pt thin films at 650°C . Nevertheless, these Pt thin films often have a poor adhesion to SiO_2/Si substrate. Akai *et al.* [35] used a $\gamma\text{-Al}_2\text{O}_3(100)$ film as a buffer layer on silicon substrate to deposit Pt thin film using rf-magnetron sputtering at low deposition rate, and they obtained highly (200)-oriented Pt thin film at 600°C . Nevertheless, this $\gamma\text{-Al}_2\text{O}_3(100)$ buffer layer was deposited on silicon substrate in high vacuum by chemical vapor deposition and high temperature (960°C). The main drawback is that these temperatures are higher than 500°C , which is most often the limit in the industrial manufacture of electronic Si-based chips. This leads to a limitation in the use of platinum electrodes which should therefore only be deposited at the early beginning of any process, especially if the (200) orientation is required. There is thus a requirement for a buffer layer to promote the deposition of (200)-oriented Pt films on silicon substrates at relatively low temperature.

In 2008, the use of oxide nanosheets (ns) as buffer layer was initiated by Kikuta *et al.* [36], and by Shibata *et al.* [37,38]. These authors showed that two-dimensional materials such as oxide nanosheets promote the growth of functional oxide materials on silicon or glass. The advantages of nanosheets are their low cost and their easy deposition by Langmuir-Blodgett method without high-vacuum set-up. Over the last twelve years, a wide variety of oxides such as SrTiO_3 , TiO_2 , ZnO , PZT, $\text{La}_{0.7}\text{Sr}_{0.3}\text{MnO}_3$, BiFeO_3 and KNbO_3 have been deposited using nanosheets of $[\text{Ca}_2\text{Nb}_3\text{O}_{10}]^-$, $[\text{Ti}_{0.87}\text{O}_2]^{0.52-}$ or $[\text{MoO}_2]^{x-}$ [16,39–44]. These ns-substrates have demonstrated their interest in obtaining well-crystallized oxide films at temperatures often lower than those usually used. For example, Nguyen *et al.* [41] showed that PZT can be deposited at only 450°C while retaining interesting ferroelectric and piezoelectric properties.

The aim of this work is to use these nanosheets buffer layers for the growth of Pt electrodes on SiO_2/Si substrate at a reasonable temperature. In a recent paper, we have shown that by using CNOs, it was possible to lower the deposition temperature of Pt thin films with (111) orientation until 200°C , while maintaining very good crystalline quality and low resistivity [45]. The objective of the present study is to explore whether the orientation control

of high quality (200)-oriented Pt electrodes on silicon substrate can be achieved using nanosheets, low deposition rate, high pressure and argon/oxygen (Ar/O₂) gas mixture. For this purpose, CNOs, with an in-plane lattice parameter (0.386 nm) close to Pt (0.393 nm), were prepared by exfoliation and deposited on silicon by Langmuir-Blodgett method. Then, Pt thin films were sputtered under different deposition conditions. These films were then characterized by X-ray diffraction (XRD), scanning electron microscopy (SEM), atomic force microscopy (AFM), and resistivity measurements.

2. Experimental methods

2.1. Materials

Boron-doped single crystalline (100) silicon samples of 7x15 mm² were used as substrates. They were coated with a 650 nm amorphous SiO₂ layer obtained by thermal growth. Pt and Ti targets with a diameter of 4 inches and a purity of 99.99% were used for sputtering thin films of Pt and TiO₂. The nanosheets were synthesized from the precursors K₂CO₃ (Acros Organics, 99 %), Ca₂CO₃ (R.P. Normapur, 99.5 %) and Nb₂O₅ (Alfa Aesar, 99.5 %).

2.2. Nanosheets synthesis

CNOs were obtained from KCa₂Nb₃O₁₀ which was synthesized by solid state reaction under the conditions of Ebina et al. [46]. An ionic exchange between potassium ions and protons was carried out using 6M HNO₃ acid during 72 hours. The acid was changed every 24 hours to obtain a powder of HCa₂Nb₃O₁₀ that was then diluted in a solution of distilled water and tetrabutylammonium hydroxide (TBA) in a 1:1 molar ratio, leading to the formation of a colloidal solution containing CNOs. This solution was then diluted and placed in a Langmuir-Blodgett (LB) trough. The SiO₂/Si substrate was first washed with distilled water and then with ethanol, before being immersed in the solution. After LB deposition of the nanosheets, the substrates were first dried at 110°C and placed under ultraviolet light to photochemically destroy TBA residues. The substrates were then air-heated at 400°C for 4 hours to remove water and organic residues from the preparation process. Finally, the stacking of the layers forming the substrate was [Ca₂Nb₃O₁₀]⁻/SiO₂/Si (CNOs/Si).

2.3. Film deposition

Platinum thin films were deposited *in situ* on CNOs(2~3 nm)/SiO₂(650 nm)/Si (CNOs/Si) and TiO₂(1~2 nm)/SiO₂(650 nm)/Si (TiO₂/Si) substrates by rf magnetron

sputtering. The sputtering targets were mounted horizontally, facing the rotating substrate holder at a distance of 4 cm. Before deposition, the targets were pre-sputtered during 15 minutes.

For the preparation of TiO₂/Si substrates, TiO₂ was rf sputtered from a metallic Ti target at 500°C. The power density was 1 W/cm², and a gaseous mixture of Ar (85 %) and O₂ (15 %) was introduced into the chamber at a pressure of 1.5 Pa. The heating and cooling ramps were 15°C/min and 30°C/min, respectively, with a 30 min-dwell time at the selected temperature before deposition starts. The deposition rate of TiO₂ was determined by measuring with SEM the thickness of several cross sections of a TiO₂ thin film deposited for 2 hours in the same conditions. The deposition time of the TiO₂ seed layer was then monitored to achieve a thickness of about 1-2 nm.

Pt thin films were then sputtered from a Pt target using a power density between 0.4 and 1 W/cm². The total pressure was tuned between 0.6 and 1 Pa, and these conditions resulted in a deposition rate varying between 2 and 20 nm/min. For all samples, the film thickness was kept close to 100 nm. Pure argon (Ar) or a mixture of Ar and oxygen (O₂) was used for sputtering, depending on the desired crystallographic orientation of the Pt film. The substrate temperature was varied from 30°C (RT) to 625°C.

2.4. Characterizations

The crystalline structure of the films was analyzed by XRD with a D8 Discover Bruker diffractometer configured in θ -2 θ reflection mode (Cu(K α) wavelength, $\lambda = 0.154056$ nm). All the measurements were calibrated against the 400 peak of the substrate (Si) and the intensity of the Pt peaks, normalized to that of the Si peak referred to as normalized intensity (nor. intensity). Rocking curves were performed on *hhh* and *h00* Pt peaks to obtain their full width at half maximum (FWHM) and so to evaluate the grain misalignment.

Contact angle measurements were performed on the different substrates with a Drop Shape Analyzer DSA 25-KRÜSS GmbH. The wetting properties of substrates were measured at RT by the static sessile drop method with a liquid droplet volume of $V = 1 \mu\text{L}$. With this method, the contact angle is given from the tangent to the solid-liquid-vapor triple point, evaluating the drop shape with the Young's equation. Five testing liquids were used: water, glycerol, formamide, ethyleneglycol and diiodomethane. The Owens-Wendt method [47] was employed to determine the surface energy of the different substrates used in this study.

The cross-sections were prepared in a DualBeam (DB) system (FEI-HELIOS 600, Elstar Field Emission SEM column and Tomahawk Focused Ga Ion Beam column) allowing both SEM characterization and the preparation of site-specific cross sections using Ga⁺ Focused Ion Beam. Before milling the cross-section, a Pt-protective layer (named Pt-DB in the following) was deposited on the area of interest using the electron beam (5 kV, 800 pA current) for the first hundred nanometers, and then the Ga⁺ ion beam (30 kV, 230 pA) for the remaining 1.4 μm . SEM observations were performed at 5 kV, with electron beam current of 400 pA and the In-Column Detector (ICD). The ICD detected Back-Scattered Electrons which were scattered very close to the electron beam axis and provided high Z-contrast signal but also a channeling effect.

A Pico SPM-LE AFM from Molecular Imaging was used in tapping mode to study the surface morphology of the samples before and after Pt deposition. In order to determine the substrate coverage by nanosheets, AFM images (obtained before Pt deposition) were analyzed using the open-source software ImageJ 1.45s (developed by NIH, version 1.45). Brightness and threshold function were adjusted to separate the areas of the substrate covered by nanosheets from the uncoated areas in two colors. AFM was also used to determine grain size and average roughness of Pt thin films. The root mean square (rms) values of the average roughness was calculated using Gwyddion (version 2.47) software from 5 μm^2 areas.

The resistivity measurements were carried out at RT using the four probes method. First, the Pt thin films were etched by Ar atoms, with an etching rate of about 35 nm/min, in order to obtain bars of 2 mm long and 150 μm , 100 μm or 50 μm width. Then, Pt plots were sputtered at RT on these bars, using lift-off. The distance between the voltage contacts was 300 μm . The measuring current was supplied by a Marconi Adret 103A current source and the voltage was recorded using a Schlumberger 7150+ digital multimeter. The current was varied from 1 to 20 μA to verify the good linearity of the voltage. The measuring current was varied from 1 to 20 μA to verify the good linearity of the recorded voltage at RT. With the 150 μm wide microbridge and a typical Pt film thickness of 100 nm, a current of 1.5 μA corresponded to a current density of 10 A/cm^2 . The resistivity uncertainty was between 1 and 1.5 $\mu\Omega\cdot\text{cm}$ and rounded to 2 $\mu\Omega\cdot\text{cm}$ for simplicity.

3. Results and discussion

3.1. Influence of deposition gas ratio on Pt crystallization and morphology

Figure 1.a shows a schematic drawing of the sample preparation from raw substrate to thin film deposition as described in the experimental section. A typical AFM image of a sample annealed in air at 400°C for 4 hours, and a height profile measured along the white line on AFM image, are given in figures 1.b and 1.c respectively. SiO₂/Si substrates present a coverage rate by CNOs above 90% (figure 1.b), which is the minimum value used in this study. The monolayer thickness of CNOs was around 2 to 3 nm and their lateral size varying from 0.5 up to 2 μm (figure 1.c). These dimensions are similar to those found by Li *et al.* [48].

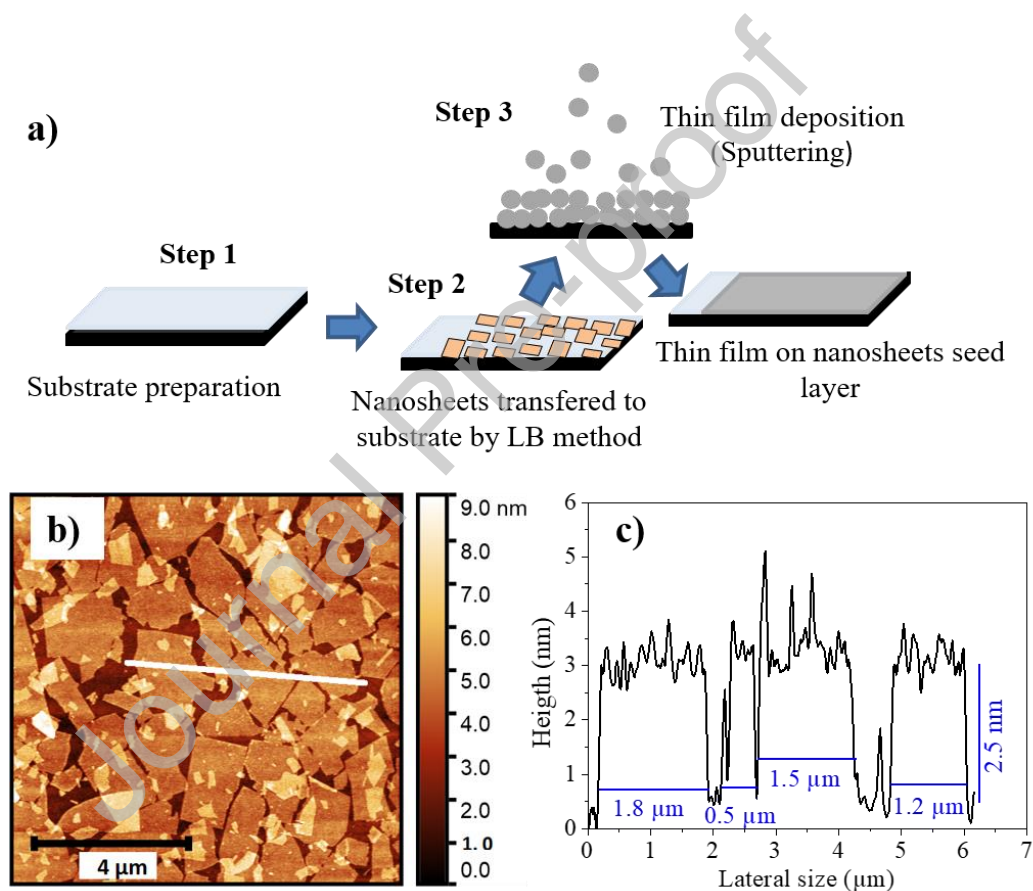


Figure 1: a) Schematic description of the deposition of nanosheets and of Pt thin films, b) AFM image of nanosheets on silicon after annealing at 400°C, and c) height profile measured on the white line drawn in b).

As we have shown in our previous study [45], the deposition of Pt thin films on CNOs/Si and TiO₂/Si substrates with a low pressure (0.6 Pa) of pure Ar led to an only (111)

orientation regardless of the growth temperature (see figure 2). 200 or 220 peaks did not appear at all. A low Full Half at Width Maximum (FWHM) of 1.05° was obtained at 200°C , indicating that CNOs allows to reduce the temperature deposition of Pt thin films on Si substrate [45]. Note that in this previous study, CNOs/Si substrates were air-heated at 300°C for 1 hour while in this study, they were air-heated at 400°C for 4 hours. This higher temperature allows for better removal of organic residues. This new thermal treatment does not change the orientation and the crystalline quality of the films grown under pure Ar at 0.6 Pa and 1 W/cm^2 .

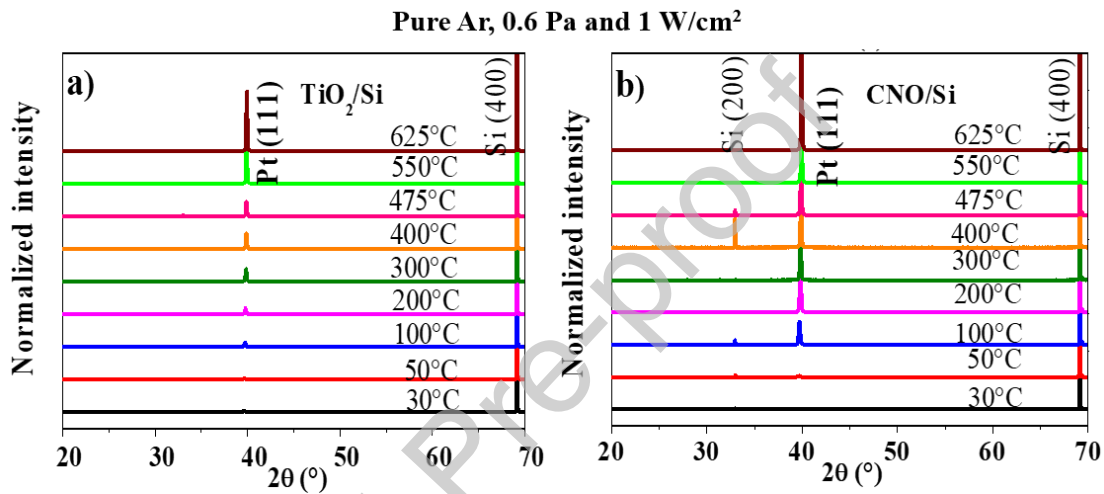


Figure 2: XRD θ - 2θ scans of Pt thin films grown at different deposition temperatures on a) TiO_2/Si substrates and b) CNOs/Si substrates under pure Ar atmosphere ($p = 0.6\text{ Pa}$) and 1 W/cm^2 power density. Figure 2 reproduced from reference [45].

This unique (111) orientation on both substrates under standard conditions was expected because metals with face-centered cubic structure like Pt have a minimum surface energy in the (111) plane. In case of bulk Pt, the surface energy for each plane is γ_{111} (977 mJ/m^2) $<$ γ_{100} (1286 mJ/m^2) $<$ γ_{110} (1553 mJ/m^2), where γ_{hkl} represents the surface energy of the (hkl) surface [29]. So, considering only the surface energy, the film is more stable if (111) oriented. However, we modified the deposition conditions to change the Pt film orientation. These different deposition conditions (named adaptive conditions in the following) were a sputtering pressure of 1 Pa, a gas mixture of 90% Ar / 10% O_2 , and a low sputtering power density of 0.4 W/cm^2 (table 1). These conditions are an optimized mixture of those reported in the literature adapted to our sputtering chamber [32–34,49–51]. It is also

possible to change the orientation of Pt films by varying its thickness [34,52], but we chose in this study to keep the thickness constant.

	Pt under standard conditions	Pt under adaptive conditions
Gas	Pure Ar	Ar 90% + O ₂ 10%
Total pressure	0.6 Pa	1 Pa
Sputtering power	1 W/cm ²	0.4 W/cm ²
Pt thickness	100 nm	100 nm
Deposition temperature	RT up to 625°C	RT up to 625°C

Table 1: Experimental conditions to obtain (111) and (200) orientations of Pt.

Figure 3 shows XRD patterns of Pt thin films deposited under adaptive conditions on both substrates as a function of the deposition temperature. It shows that when Pt thin films were deposited on CNOs/Si at a deposition temperature below 500°C, (111) oriented Pt was obtained with only a weak 200 peak at 500°C. The intensity of this 200 peak then increases with the deposition temperature while the intensity of the 111 peak decreases, indicating that Pt film changes its orientation from (111) at low temperature toward (200) at high deposition temperature. For all these temperatures, only the 111 Pt peak was observed on TiO₂/Si substrate despite using adaptive conditions. This is due to the deposition temperature which is not sufficient to crystallize other orientations of Pt on this substrate. Indeed, the change of the orientation of Pt thin film from the (111) plane toward the (200) plane on silicon substrate, in addition to the use of adaptive conditions (high pressure, high thickness, low sputtering power, Ar/O₂ gas mixture), requires very high deposition temperatures, typically above 750°C [32,33]. The XRD results presented in figure 3 clearly shows that the CNOs play a key role on the crystallization of Pt (200) orientation on silicon substrate, at moderate deposition temperature and with adaptive conditions. Note that on some patterns, the forbidden Si 200 reflection is present. This phenomenon, known as "Umweganregung", is a multiple diffraction event depending on the in-plane orientation of the sample [53].

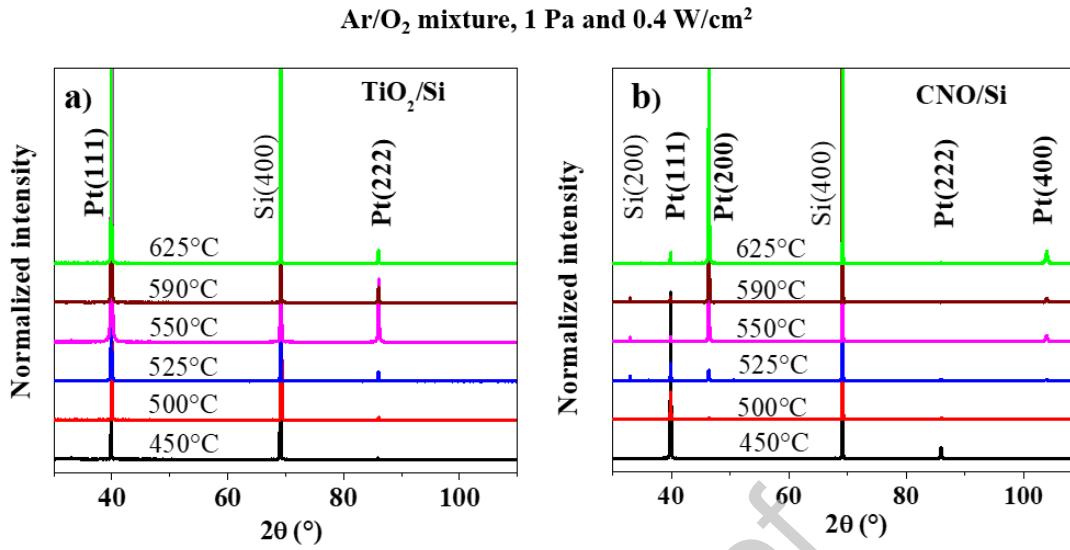


Figure 3: XRD θ - 2θ scans of Pt thin films grown at different deposition temperatures under adaptive conditions on a) TiO₂/Si substrates and b) CNOs/Si substrates. Deposition atmosphere was composed of Ar 90% and O₂ 10%, at a pressure of 1 Pa, and a low sputtering power density of 0.4 W/cm² was used.

To go further, figure 4.a shows the intensity fraction of 200 Pt peak (f_{200}) as a function of deposition temperature, calculated from the equation:

$$f_{200} = \frac{2 I_{200}}{I_{111} + 2 I_{200}} \times 100 \quad (1)$$

where I_{111} and I_{200} are the intensities of 111 and 200 Pt peaks respectively. The factor 2 takes into account the X-Ray powder diffraction pattern of the bulk Pt [54]. It can be seen that the (111) orientation is dominant below 500°C on CNOs substrates. Above 500°C, the film orientation begins to switch from (111) to (200), and highly (200) oriented films were achieved from 550°C. This is in good agreement with the results for Pt thin films deposited on single crystal MgO substrate by PLD and sputtering [49,55].

The influence of the deposition temperature on the FWHM of the rocking-curve of Pt 200 and 111 peaks, for films deposited on CNOs/Si substrate, is reported on figure 4.b. The FWHM indicates the degree of misalignment of the crystallites relative to the normal of the film plane. At temperatures above 550°C, the (200) oriented films are well crystallized and the FWHM is below 0.8°. As the substrate temperature decreases to 450°C, the FWHM of the

200 peak increases while the FWHM of the 111 peak decreases, which means that a gradual alignment of the crystallites along the (111) planes is achieved by reducing the temperature.

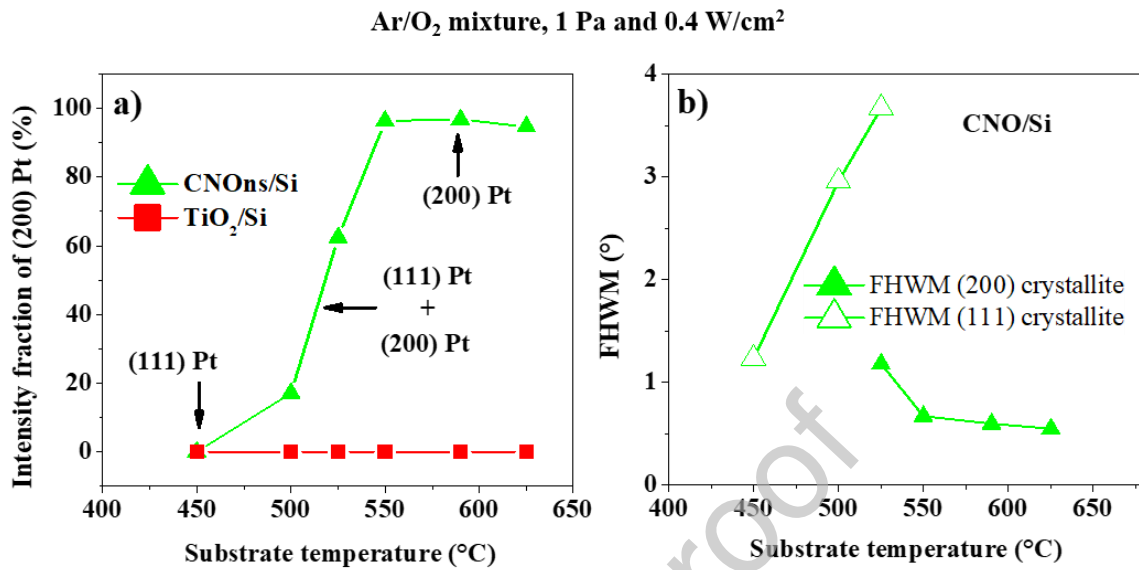


Figure 4: Influence of the deposition temperature on a) the intensity fraction of (200) Pt and b) the FWHM of the rocking curve of 200 and 111 peaks for Pt films deposited on CNOs/Si substrates under adaptive conditions. The FWHM of the rocking curve of 200 peak at 500°C and 111 peak above 525°C are not shown because these peaks are very broad and have very low intensities. Deposition atmosphere was composed of Ar 90% and O₂ 10%, at a pressure of 1 Pa, and a low sputtering power density of 0.4 W/cm² was used.

We have shown in our previous study [45], that the coverage of CNOs on SiO₂/Si substrate is not a crucial parameter for the deposition of high quality (111) Pt thin films at low temperature. Under adaptive conditions, with CNOs coverage ranging from 30% to 96%, the orientation of Pt films linearly turns from mainly (111) for low covered substrates to almost fully (002) at high coverage (Figure 5 a) and b)). This indicates that Pt films are (200) oriented only on the areas of the substrate covered with CNOs and remain (111) oriented on the uncovered parts of the substrate. The CNOs coverage is therefore selective for the orientation of Pt films on CNOs/Si, confirming that nanosheets play a key role in the orientation control of Pt films.

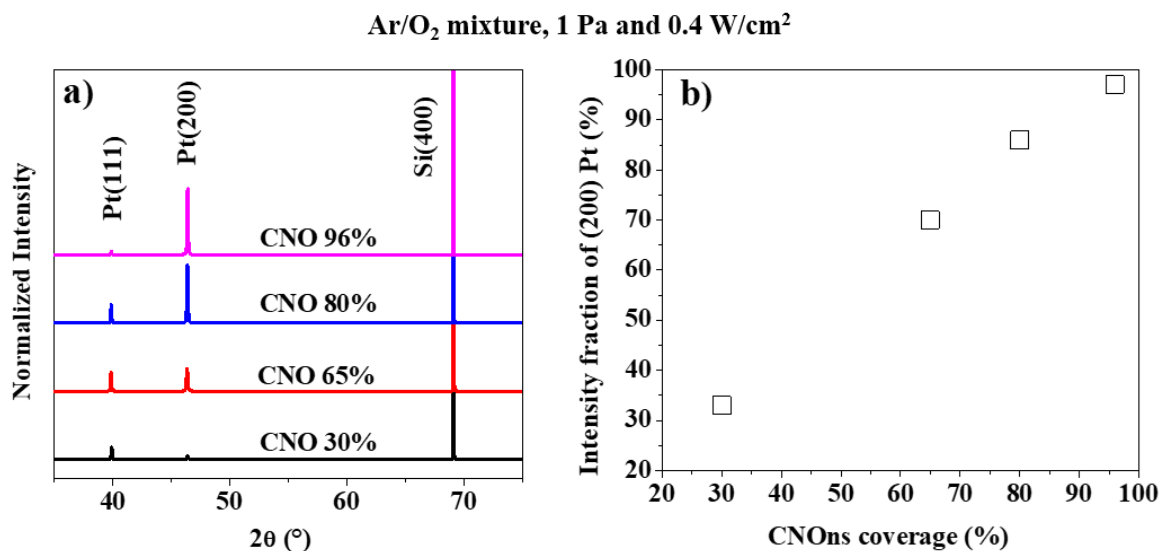


Figure 5: a) XRD θ - 2θ scans of Pt thin films grown at 600°C under adaptive conditions on CNOs/Si substrates with different CNOs coverage, b) influence of the ns coverage on the intensity fraction of (200) Pt. Deposition atmosphere was composed of Ar 90% and O₂ 10%, at a pressure of 1 Pa, and a low sputtering power density of 0.4 W/cm² was used.

Figure 6.a shows the evolution of the Pt lattice parameter as a function of the substrate temperature in the range of 400 to 625°C, for films deposited on CNOs/Si and TiO₂/Si under standard or adaptive conditions. For this range of growth temperature, the lattice parameter is lower than the bulk one (0.3928 nm) and decreases with increasing growth temperature. This indicates that the films are in a tensile stress in their plane. However, the lattice parameter of films deposited under Ar/O₂ gas mixture is larger than that of the films deposited under pure Ar atmosphere. It is even more noticeable above 500°C where (200) Pt orientation is obtained on CNOs, meaning that oxygen, and perhaps sputtering power, in adaptive conditions, decreases the tensile stress in the Pt thin films deposited at high temperature. Similar results were obtained by Kim *et al.* [56] for Pt thin films deposited on SiO₂/Si substrates under Ar/O₂ gas mixtures. These authors speculated that this tendency to decrease the tensile stress in the Pt thin films is due to the incorporation of oxygen into grain boundaries. It has been shown in various metal systems that increasing compressive stress, decreasing tensile stress, or minimizing surface and interface energies can lead to a change of their texture and orientation [56–60]. In our case, figure 6.a shows that the decrease in tensile stress is observed on both CNOs/Si and on TiO₂/Si, and thus it does not explain why the change of orientation is

obtained only on CNOs. Therefore, we will discuss later the contribution of the surface energy of the seed layers on the orientation change of Pt thin films.

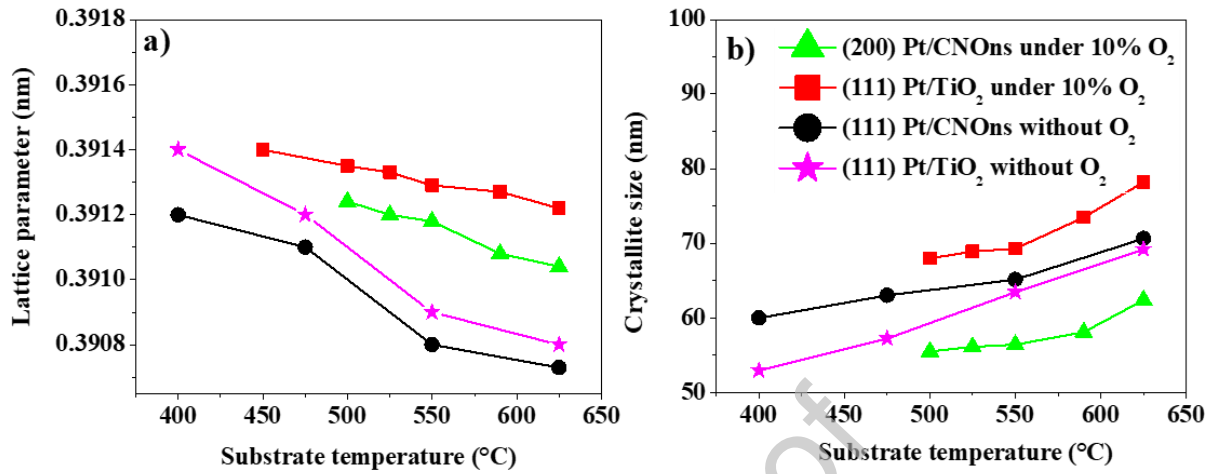


Figure 6: Evolution of the lattice parameter (a) and of the crystallite size (b) as a function of the deposition temperature of thin films deposited with 10% O₂ and without O₂. For 10% O₂, deposition atmosphere was composed of Ar 90% and O₂ 10%, at a pressure of 1 Pa, and a low sputtering power density of 0.4 W/cm² was used. In case without O₂, deposition atmosphere was pure Ar at a pressure of 0.6 Pa, and the sputtering power density was 1 W/cm².

Figure 6.b shows the evolution of the crystallite size with and without O₂ as a function of the substrate temperature. It can be clearly seen that the crystallite size increases with the growth temperature, indicating that a better crystallization occurs in the films. However, the (200) oriented crystallites are smaller in size than the (111) oriented ones, which means that the size of the crystallites probably depends on the orientation of the film.

According to the theory of the nucleation and growth of thin films, one of the parameters that determines the growth model (texturation and orientation) is the surface-interface balance energy between the film and the substrate [61–64]. To evaluate the contribution of the substrate surface energy on the growth and orientation of Pt thin films, we studied the wettability and determined the surface energy of CNOs/Si and TiO₂/Si substrates, using contact angle measurements. The surface energy of silicon without seed layer (SiO₂/Si) was also determined for comparison. The contact angle is given by using the sessile drop method with the Young's equation:

$$\cos(\theta) = \frac{\gamma_s - \gamma_{sl}}{\gamma_l} \quad (2)$$

where θ is the contact angle, and γ_s , γ_{sl} and γ_l are the surface energies of the substrate, the substrate-liquid interface and the liquid respectively. Water, glycerol, formamide, ethylene glycol and diiodomethane were used to investigate wettability. Figure 7 shows the variations of the contact angle with the liquids and substrates. For four liquids, we found that the lowest contact angle were measured for the CNOns/Si substrate compared to other TiO_2/Si and SiO_2/Si substrates, indicating that a better wettability is achieved with the CNOns seed layer. Water gave also the highest difference in contact angle between the TiO_2/Si and SiO_2/Si substrates.

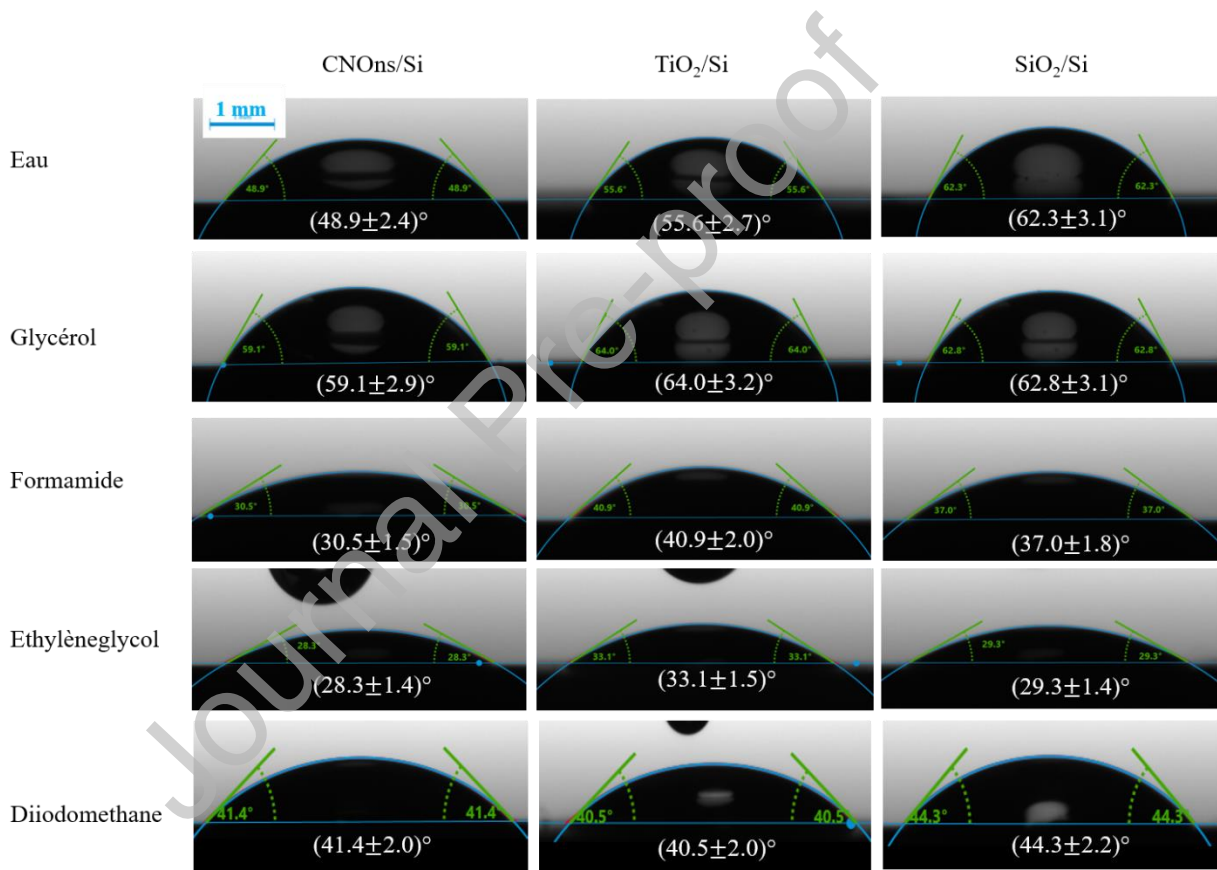


Figure 7: Variation of the contact angle of different testing liquids on CNOns/Si, TiO_2/Si and SiO_2/Si substrates.

To determine the surface energy of the substrates, the Owens-Wendt method [47] was used. This method considers the geometric mean of the dispersive (γ^d) and polar (γ^p) parts of the surface tension of the liquids and of the surface energy of the solids (eq3):

$$\gamma_{sl} = \gamma_s + \gamma_l - 2\sqrt{\gamma_s^d \gamma_l^d} - 2\sqrt{\gamma_s^p \gamma_l^p} \quad (3)$$

Substituting (eq3) in (eq2), a linear equation of the type $y = ax + b$ (eq4) is obtained:

$$\frac{\gamma_l(1+\cos(\theta))}{2\sqrt{\gamma_l^d}} = \sqrt{\gamma_s^p} \sqrt{\frac{\gamma_l^p}{\gamma_l^d}} + \sqrt{\gamma_s^d} \quad (4)$$

where $y = \frac{\gamma_l(1+\cos(\theta))}{2\sqrt{\gamma_l^d}}$ and $x = \sqrt{\frac{\gamma_l^p}{\gamma_l^d}}$ contain the known parameters, namely the measured

contact angle, and the dispersive γ_l^d and polar γ_l^p parts of the liquid surface tension for each liquid. The linear regression of (eq4) leads directly to the components of the solid surface energy: $\gamma_s^p = a^2$ and $\gamma_s^d = b^2$ with $\gamma_s = \gamma_s^p + \gamma_s^d$ (see figure 8 and Table 2 for results). As can be seen, the highest surface energy of 47.8 mJ/m² was obtained for CNOs/Si substrate. No significant difference was observed for TiO₂/Si and SiO₂/Si substrates with surface energies of 42.7 and 40.9 mJ/m², respectively. These surface energy values are similar to those reported by other authors on seed layer (tantalum) or oxide substrates [62,64]. This result clearly shows that the CNOs seed layer increases the surface energy compared to the SiO₂/Si substrate. This can contribute to the nucleation and the growth of (200) oriented crystallites when oxygen and low sputtering power are used under adaptive conditions. This hypothesis can also explain the high crystalline quality of (111) Pt thin films obtained using CNOs/Si substrates at low deposition temperature (200°C and rocking curve = 1.05°) [45]. Thus, the increase of the surface energy is an important way in order to increase the nucleation, growth and texturation of thin films [62,64]. Note that our study of the surface energies was carried out at room temperature for all the substrates, and we assume that the surface energies evolve similarly with temperature. The same reasoning has been used to explain the nucleation of 15R-SiC and LiNbO₃ films on different substrates [62,64].

Substrate	Surface energy (mJ/m ²)		
	γ_s^d	γ_s^p	γ_s
SiO ₂ /Si	21.4 ± 1.0	19.5 ± 1.0	40.9 ± 2.0
TiO ₂ /Si	18.2 ± 0.9	24.5 ± 1.2	42.7 ± 2.1
CNOs/Si	17.5 ± 0.8	30.3 ± 1.5	47.8 ± 2.3

Table 2: Values of surface energy for each substrate deduced from contact angle measurement using the Owens-Wendt method.

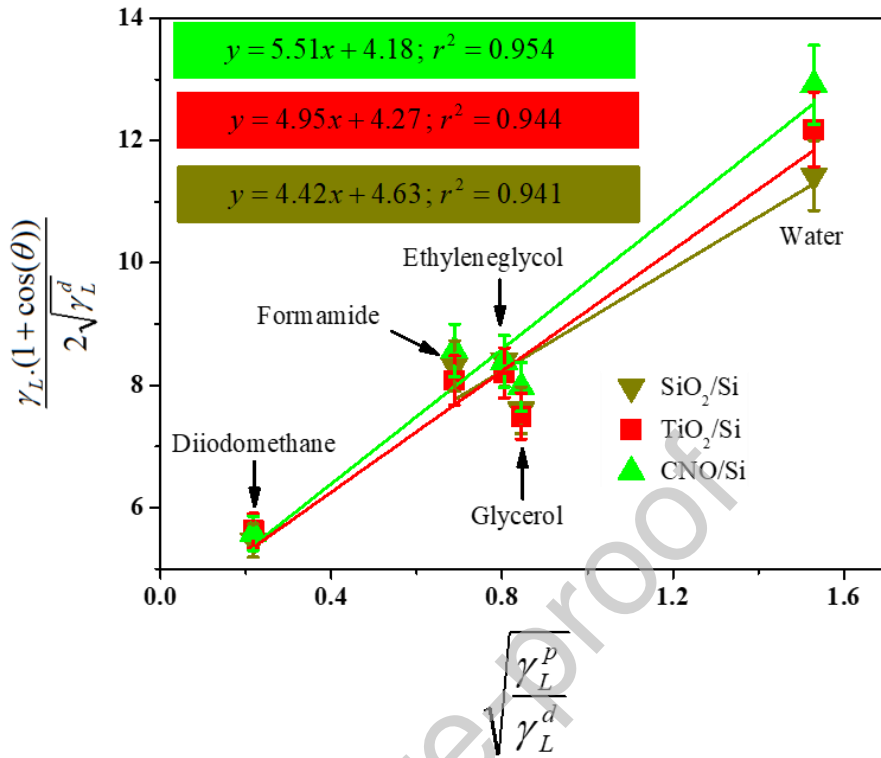


Figure 8: Linear regression of the Owens-Wendt equation obtained for different liquids and substrates.

Figures 9 and 10 show the AFM images and surface topography of Pt films deposited at different temperatures with the adaptive conditions on CNOs/Si and TiO₂/Si. It shows that the surface topography and grain morphology change with the film orientation. Smoother surfaces with a rms roughness of 6 to 7 nm are obtained for pure (200) orientation at high temperatures, while the rms roughness is greater than 10 nm for (111) films deposited at low temperatures (figure 9). On the other hand, the surface roughness of (111) Pt is approximately the same on CNOs/Si and TiO₂/Si (compare figures 9 and 10, 500°C and 525°C). This indicates that the surface roughness depends mainly on the film orientation when the adaptive conditions are used. However, the rms surface roughness of the films deposited under standard conditions (thus with only the (111) orientation) was much lower and around 1 to 2 nm on both substrates [45]. This difference on the surface roughness may result from the addition of O₂, lower sputtering power, or higher pressure under the adaptive conditions. These conditions could then decrease the mobility of Pt atoms at the surface of the substrates and thus change the roughness of these films. For example, Lee et al. showed that O₂ can

incorporate in Pt grain boundaries or lattice to form platinum oxide and alter its morphology and grains size [33].

(200) and (111) Pt on CNOs/Si under Ar/O₂ mixture, 1 Pa and 0.4 W/cm²

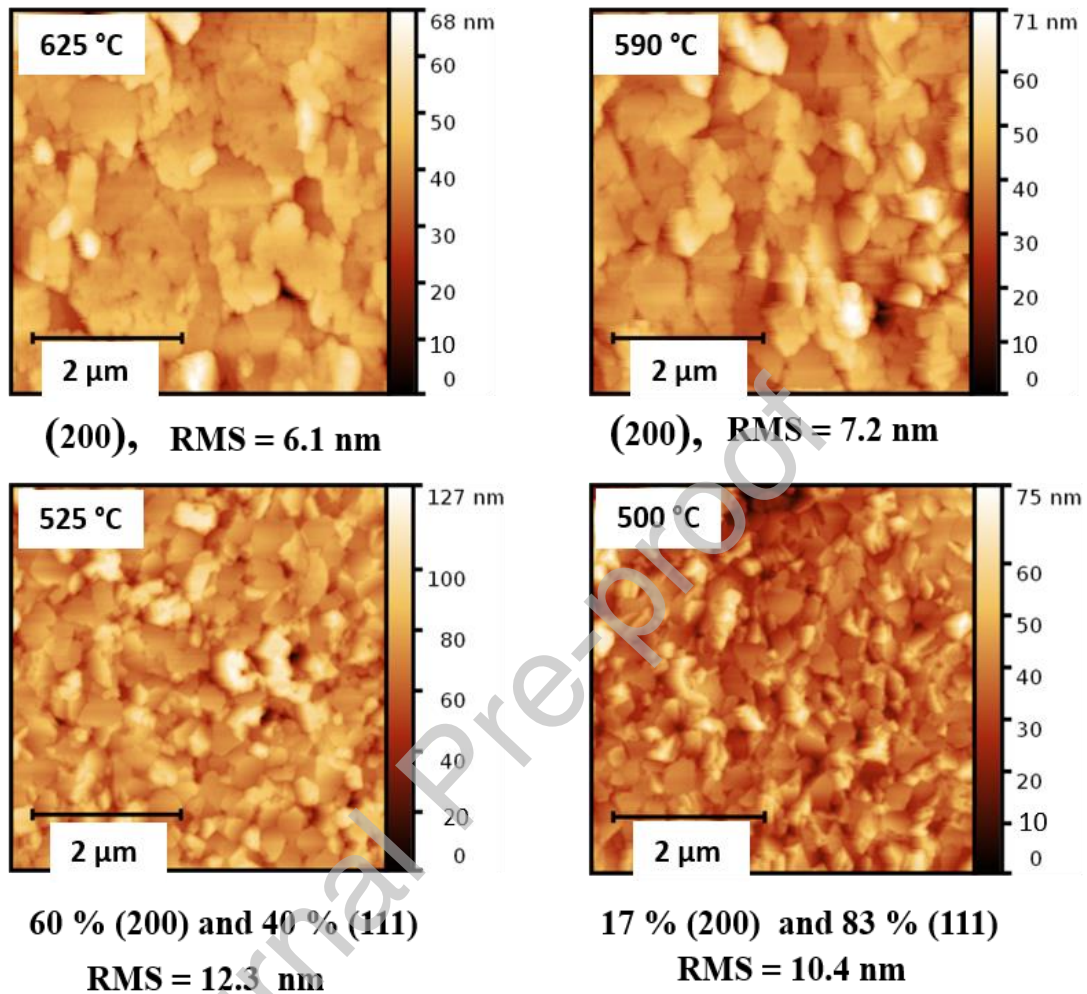


Figure 9: AFM images of Pt films deposited on CNOs/Si at different temperatures and under adaptive conditions, with (200) and (111) orientations. Deposition atmosphere was composed of Ar 90% and O₂ 10%, at a pressure of 1 Pa, and a low sputtering power density of 0.4 W/cm² was used.

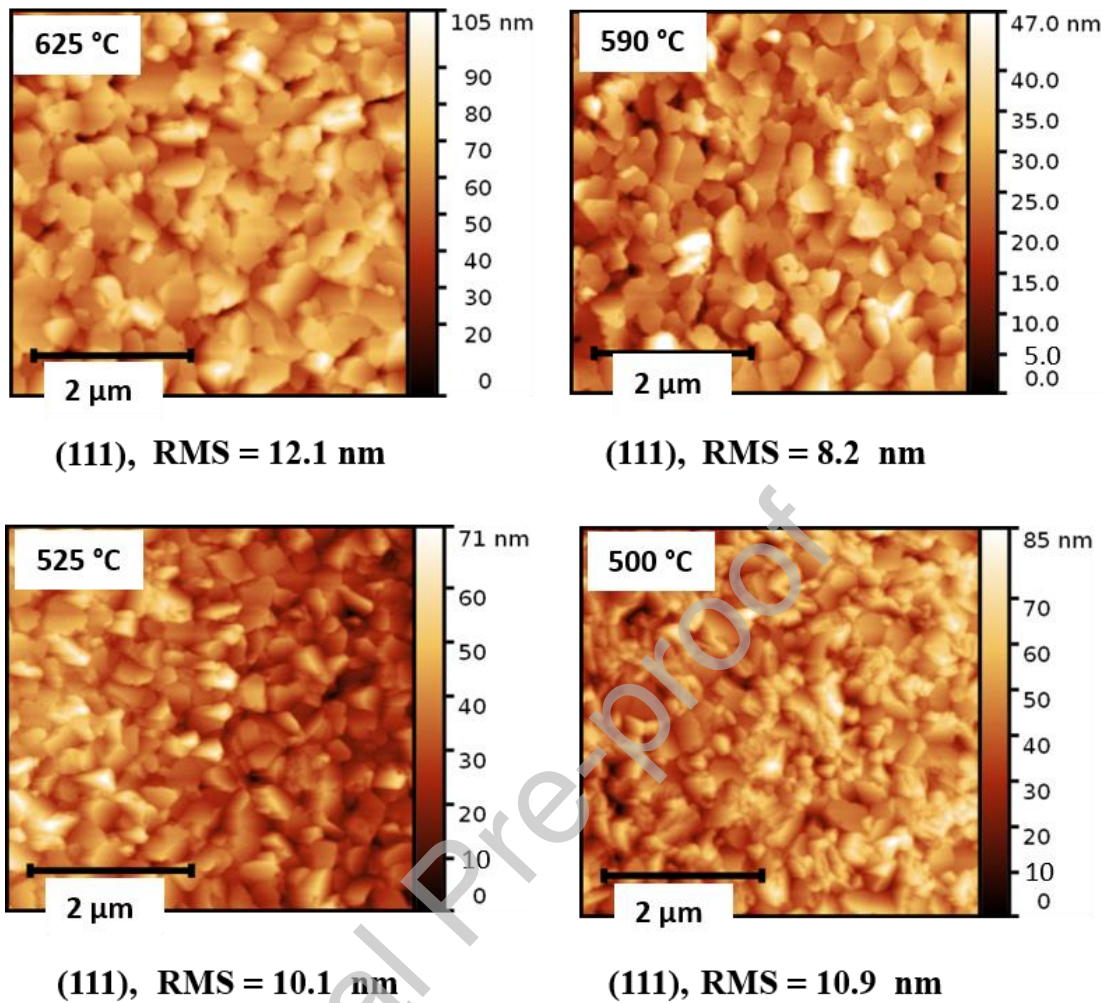
(111) Pt on TiO₂/Si under Ar/O₂ mixture, 1 Pa and 0.4 W/cm²

Figure 10: AFM images of (111) Pt films deposited on TiO₂/Si at different temperatures under adaptive conditions. Deposition atmosphere was composed of Ar 90% and O₂ 10%, at a pressure of 1 Pa, and a low sputtering power density of 0.4 W/cm² was used.

Figure 11 shows SEM images of cross-sections prepared from Pt films grown on CNOs/Si substrates at different deposition temperatures under the adaptive and standard conditions. The films deposited under the adaptive conditions have a non-uniform surface morphology with the presence of hollows at the grain boundaries and a variation of the thickness (figure 11.a). This may be due to the high pressure or the addition of oxygen in the sputtering gas. In contrast, as we have shown in our previous study [45], thin films deposited under standard conditions have a uniform surface morphology and an almost constant thickness (figure 11.b)). These observations are in agreement with the AFM results : the films under standard conditions have a lower roughness than those under the adaptive conditions.

The SEM images also show that the microstructure of the films varies with the temperature and the presence of oxygen. As can be seen in Table 3, the thickness of the thin films under the adaptive conditions varies greatly, and the change is more noticeable when the deposition temperature decreases. For example, the thickness varies between 90 to 110 nm at 625°C and from 95 to 140 nm (for a few grains) at 450°C. The film at 625°C has large grains of 70 to 400 nm, and the grains size decreases with deposition temperature. For the films under standard conditions, the 625°C film with a thickness of 100 nm has large grains of 50-200 nm, but less than the 625°C film under the adaptive conditions. The film at RT with a thickness of 90 nm has very small grains (only several tens of nanometers wide). All these observations show that the effect of high pressure, low power or incorporation of oxygen in these films largely change their morphology and their grains size.

	Deposition temperature (°C)	Thickness (nm)	Grains size (nm)
Appropriate conditions	625	90-110	70-400
	525	70-120	50-100
	500	80-115	35-150
	450	95-140 (few grains)	20-100
Standard conditions	625	100	50-200
	30	90	Few tens of nm

Table 3: Summary of the SEM microstructural characterizations of Pt thin films on CNOs/Si under standard and adaptive conditions.

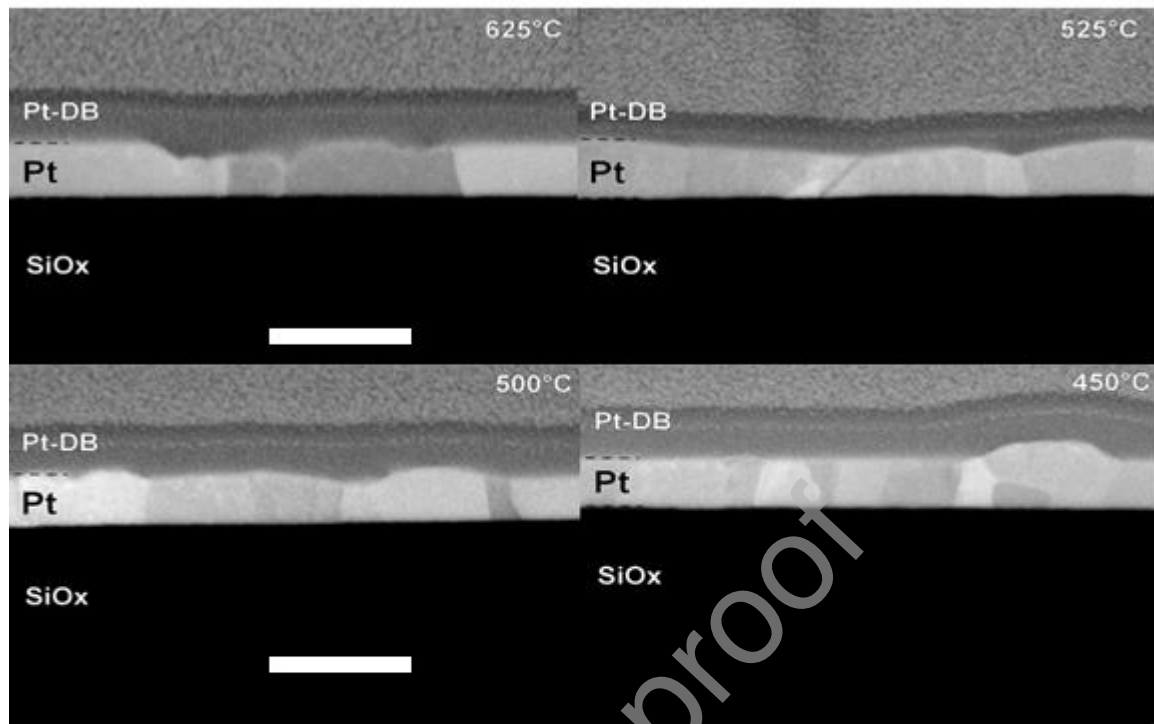
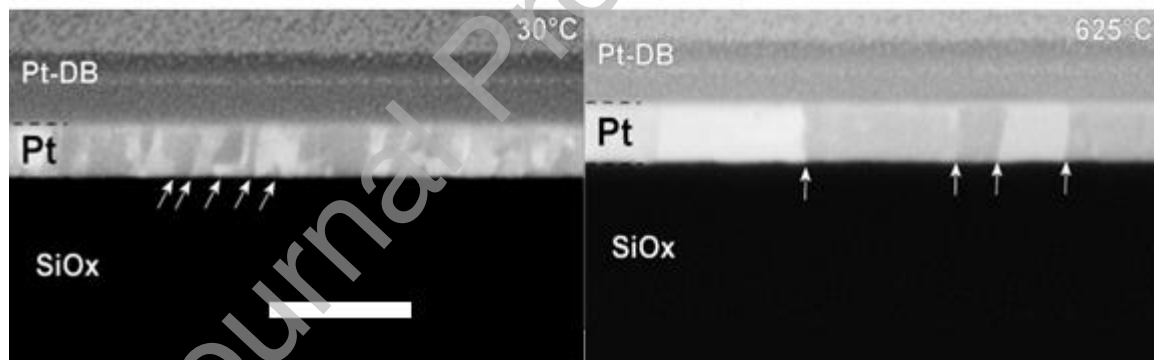
a) Pt/CNO/Si under Ar/O₂ mixte, 1 Pa and 0.4 W/cm²b) Pt/CNO/Si under pure Ar, 0.6 Pa and 1 W/cm²

Figure 11: SEM images of Pt films grown on CNOs/Si substrates at different temperatures under a) adaptive conditions and b) standard conditions. Arrows highlight differences in grain size. Tilt angle is 52°. Pt-DB refers to the protective Pt-based film deposited in the DualBeam system. The white bar represents 200 nm. Figure 11.b) reproduced from reference [45]. For figure 11.a), deposition atmosphere was composed of Ar 90% and O₂ 10%, at a pressure of 1 Pa, and a low sputtering power density of 0.4 W/cm² was used. In case without figure 11.b), deposition atmosphere was pure Ar at a pressure of 0.6 Pa, and the sputtering power density was 1 W/cm².

3.2. Influence of deposition atmosphere on the Pt resistivity

The resistivity of thin films is generally greater than that of the bulk platinum (10.6 $\mu\Omega\cdot\text{cm}$). Table 4 shows the resistivity values of the Pt thin films deposited at different deposition temperatures under standard conditions (with pure Ar) and adaptive conditions (with Ar/O₂ gas mixture) on both types of substrates. The Pt thin films deposited under adaptive conditions show lower resistivity values of 13 to 20 $\mu\Omega\cdot\text{cm}$ than those deposited under standard conditions with pure Ar, for which the resistivity values were 18 to 24 $\mu\Omega\cdot\text{cm}$. This decrease in resistivity of Pt thin films under oxygen ambient could be due to the presence of larger grains in the films as observed in SEM images (Table 3). Similar results were observed by Lee *et al.* [33] for Pt thin films (1 μm thick) deposited on TiO₂/SiO₂/Si substrates by magnetron sputtering. Slightly lower resistivity values (10.7 to 12.7 $\mu\Omega\cdot\text{cm}$) were obtained for Pt films with giant grains, deposited under oxygen ratio of 2.5 to 10% and annealed at temperatures above 750°C. Qiu *et al.* [65] also obtained a smaller resistivity value of 1.5 $\mu\Omega\cdot\text{cm}$ with 15% of oxygen, while a resistivity value of 29.4 $\mu\Omega\cdot\text{cm}$ was obtained under pure Ar for 150 nm thick Pt films deposited on MgO substrate by magnetron sputtering at a temperature of 700°C. Oxygen incorporation into Pt films can change the deposition rate, stress, surface morphology, grain size, orientation, and resistivity. Other authors have observed that the addition of oxygen into a Pt thin film increases its resistivity due to the formation of platinum oxide [56,66]. On the other hand, this study shows that there is no significant difference in resistivity for the two types of seed layers as a function of temperature under an argon/oxygen gas mixture or with pure argon.

	Substrate	Substrate	Pt film thickness	Resistivity
--	-----------	-----------	-------------------	-------------

		temperature (°C)	(nm)	($\mu\Omega.cm$)
Pt films under pure Ar	CNOs/Si	625	100	18
		30	90	24
	TiO ₂ /Si	625	110	20
		30	95	22
Pt films under Ar+O ₂	CNOs/Si	625	90-110	13 to 16
		450	95-140 (few grains)	13 to 20
	TiO ₂ /Si	625	90-110	14 to 17
		450	95-140 (few grains)	13 to 19

Table 4: Resistivity of Pt films deposited at different temperatures on the two kinds of substrates under pure Ar and Ar+O₂ gas mixture.

4. Conclusion

This study focused on the influence of seed layers ([Ca₂Nb₃O₁₀]⁻ nanosheets or TiO₂) and the deposition conditions on the crystallization and orientation of 100 nm thick Pt thin films deposited on silicon. For Pt thin film deposited with pure argon, XRD, AFM and SEM imaging characterizations showed that the CNOs seed layer gave better crystallization of Pt thin films. The FWHM of the 111 Pt peak remains very low, even at low temperatures, *i.e.* 1.05° at 200°C, indicating that the CNOs allow a significant reduction of the deposition temperature of Pt thin films on Si substrate. The addition of oxygen during deposition under adaptive conditions leads to a change of the orientation of Pt films, from (111) to fully (200), only on the CNOs seed layer, and above 550°C. Furthermore, oxygen addition, low sputtering power and high pressure change the surface morphology, roughness, grain size and resistivity of the Pt thin films deposited on the CNOs and TiO₂ seed layers. Slightly lower resistivity values of 13 to 20 $\mu\Omega.cm$ were obtained for these Pt thin films. Finally, the possibility of tuning the orientation of Pt films on silicon substrates and at fairly low temperature (550°C) thanks to nanosheets, open the perspective of a wide variety of complex oxides integration, with interesting dielectric, ferroelectric or magnetoelectric properties.

Acknowledgements

This work was carried out with the financial support of the French Agence Nationale de la Recherche (ANR-17-CE08-0012) as part of the POLYNASH project and with the financial support of the program EQUIPEX GENESIS (ANR-11-EQPX-0020) for the preparation of cross-section and the SEM study.

Authors declare no conflict of interest.

Declaration of interests

The authors declare the following financial interests/personal relationships which may be considered as potential competing interests:

Arnaud Fouchet reports financial support was provided by French Agence Nationale de la Recherche (ANR-17-CE08-0012). B. Domenges reports financial support was provided by EQUIPEX GENESIS (ANR-11-EQPX-0020).

Credit Authors Statements:

J.J. Manguel, C. Cibert and G. Poullain carried out the manipulations such as Pt film deposition by sputtering, structural analysis by XRD, surface analysis by AFM, surface energy and resistivity measurements, and writing the paper.

F. Baudouin, V. Demange, and M. Guilloux-Viry carried out the synthesis of CNOs nanosheets and their deposition on SiO₂/Si substrates. They also wrote the paper.

B. Domengès carried out the microstructural characterizations of Pt thin film, wrote the paper and found financial support provided by EQUIPEX GENESIS (ANR-11-EQPX-0020).

A. Fouchet wrote the paper and found financial support provided by French Agence Nationale de la Recherche (ANR-17-CE08-0012).

References:

- [1] R. Takayama, Y. Tomita, Preparation of epitaxial $\text{Pb}(\text{Zr}_x\text{Ti}_{1-x})\text{O}_3$ thin films and their crystallographic, pyroelectric, and ferroelectric properties, *Journal of Applied Physics*. 65 (1989) 1666–1670. <https://doi.org/10.1063/1.342936>.
- [2] G.L. Rhun, G. Poullain, R. Bouregba, B. Vilquin, Influence of Orientation and Oxygen Content on Electrical Properties of In Situ Deposited PZT Thin Films, *Ferroelectrics*. 288 (2003) 111–120. <https://doi.org/10.1080/00150190390211954>.
- [3] G. Cui, P.C. Van Buskirk, J. Zhang, C.P. Beetz, J. Steinbeck, Z.L. Wang, J. Bentley, Epitaxial growth of Pt (001) thin films on MgO (001) under oxidizing conditions, *MRS Online Proceedings Library Archive*. 310 (1993).
- [4] S. Hiboux, P. Muralt, N. Setter, Orientation and Composition Dependence of Piezoelectric-Dielectric Properties of Sputtered $\text{Pb}(\text{Zr}_x\text{Ti}_{1-x})\text{O}_3$ Thin Films, *MRS Online Proceedings Library*. 596 (1999) 499–504. <https://doi.org/10.1557/PROC-596-499>.
- [5] W. Gong, J.-F. Li, X. Chu, Z. Gui, L. Li, Combined effect of preferential orientation and Zr/Ti atomic ratio on electrical properties of $\text{Pb}(\text{Zr}_x\text{Ti}_{1-x})\text{O}_3$ thin films, *Journal of Applied Physics*. 96 (2004) 590–595. <https://doi.org/10.1063/1.1759072>.
- [6] P. Muralt, T. Maeder, L. Sagalowicz, S. Hiboux, S. Scalese, D. Naumovic, R.G. Agostino, N. Xanthopoulos, H.J. Mathieu, L. Patthey, E.L. Bullock, Texture control of PbTiO_3 and $\text{Pb}(\text{Zr},\text{Ti})\text{O}_3$ thin films with TiO_2 seeding, *Journal of Applied Physics*. 83 (1998) 3835–3841. <https://doi.org/10.1063/1.366614>.
- [7] Y. Sakashita, H. Segawa, K. Tominaga, M. Okada, Dependence of electrical properties on film thickness in $\text{Pb}(\text{Zr}_x\text{Ti}_{1-x})\text{O}_3$ thin films produced by metalorganic chemical vapor deposition, *Journal of Applied Physics*. 73 (1993) 7857–7863. <https://doi.org/10.1063/1.353936>.
- [8] T. Hase, T. Sakuma, Y. Miyasaka, K. Hirata, N. Hosokawa, Preparation of $\text{Pb}(\text{Zr}, \text{Ti})\text{O}_3$ Thin Films by Multi-Target Sputtering, *Jpn. J. Appl. Phys.* 32 (1993) 4061. <https://doi.org/10.1143/JJAP.32.4061>.
- [9] A.K. Tagantsev, M. Landivar, E. Colla, N. Setter, Identification of passive layer in ferroelectric thin films from their switching parameters, *Journal of Applied Physics*. 78 (1995) 2623–2630. <https://doi.org/10.1063/1.360122>.

- [10] J.R. Slack, J.C. Burfoot, Electrical properties of flash evaporated ferroelectric BaTiO₃ thin films, *J. Phys. C: Solid State Phys.* 4 (1971) 898–909. <https://doi.org/10.1088/0022-3719/4/8/016>.
- [11] S.K. Dey, J.-J. Lee, P.A.P. Alluri, Electrical Properties of Paraelectric (Pb 0.72La 0.28)TiO₃ Thin Films with High Linear Dielectric Permittivity: Schottky and Ohmic Contacts, *Jpn. J. Appl. Phys.* 34 (1995) 3142. <https://doi.org/10.1143/JJAP.34.3142>.
- [12] J.J. Lee, C.L. Thio, S.B. Desu, Electrode contacts on ferroelectric Pb(Zr_xTi_{1-x})O₃ and SrBi₂Ta₂O₉ thin films and their influence on fatigue properties, *Journal of Applied Physics.* 78 (1995) 5073–5078. <https://doi.org/10.1063/1.359737>.
- [13] P.K. Larsen, G.J.M. Dormans, D.J. Taylor, P.J. van Veldhoven, Ferroelectric properties and fatigue of PbZr_{0.51}Ti_{0.49}O₃ thin films of varying thickness: Blocking layer model, *Journal of Applied Physics.* 76 (1994) 2405–2413. <https://doi.org/10.1063/1.357589>.
- [14] A.K. Tagantsev, I.A. Stolichnov, Injection-controlled size effect on switching of ferroelectric thin films, *Appl. Phys. Lett.* 74 (1999) 1326–1328. <https://doi.org/10.1063/1.123539>.
- [15] R. Bouregba, G. Poullain, Computation of the polarization due to the ferroelectric layer in a stacked capacitor from Sawyer–Tower hysteresis measurements, *Journal of Applied Physics.* 93 (2003) 522–532. <https://doi.org/10.1063/1.1527212>.
- [16] M.D. Nguyen, H. Yuan, E.P. Houwman, M. Dekkers, G. Koster, J.E. ten Elshof, G. Rijnders, Highly Oriented Growth of Piezoelectric Thin Films on Silicon Using Two-Dimensional Nanosheets as Growth Template Layer, *ACS Appl. Mater. Interfaces.* 8 (2016) 31120–31127.
- [17] Y. Minemura, D. Ichinose, K. Nagasaka, J.W. Kim, H. Shima, K. Nishida, T. Kiguchi, T.J. Konno, N. Oshima, H. Funakubo, H. Uchida, Polar-axis-oriented crystal growth of tetragonal PZT films on stainless steel substrate using pseudo-perovskite nanosheet buffer layer, *AIP Advances.* 5 (2015) 077139. <https://doi.org/10.1063/1.4927208>.
- [18] X.D. ZHANG, T. LIN, X.J. MENG, J.L. SUN, J.H. CHU, S. PARK, H. KWON, J. HWANG, G. PARK, Effect of Sputtering Working Pressure on Microstructures and Properties of Pzt Thin Films, *Integrated Ferroelectrics.* 113 (2010) 31–40. <https://doi.org/10.1080/10584587.2009.490184>.
- [19] M. Dekkers, M.D. Nguyen, R. Steenwelle, P.M. te Riele, D.H.A. Blank, G. Rijnders, Ferroelectric properties of epitaxial Pb(Zr,Ti)O₃ thin films on silicon by control of crystal orientation, *Appl. Phys. Lett.* 95 (2009) 012902. <https://doi.org/10.1063/1.3163057>.

- [20] C. Yang, M. Chen, T. Hong, C. Wu, J. Wu, T. Wu, Preparation of (100)- oriented metallic LaNiO₃ thin films on Si substrates by radio frequency magnetron sputtering for the growth of textured Pb(Zr_{0.53}Ti_{0.47})O₃, *Appl. Phys. Lett.* 66 (1995) 2643–2645. <https://doi.org/10.1063/1.113111>.
- [21] D.-H. Kuo, W.-H. Wu, C.-L. Chang, Growth and characterization of sputtered LaNiO₃ films obtained with (La₂NiO₄+Ni) cermet targets, *Thin Solid Films.* 517 (2008) 731–736. <https://doi.org/10.1016/j.tsf.2008.08.161>.
- [22] S. Zhao, F. Ma, Z. Song, K. Xu, The growth behavior and stress evolution of sputtering-deposited LaNiO₃ thin films, *Materials Science and Engineering: A.* 474 (2008) 134–139. <https://doi.org/10.1016/j.msea.2007.04.004>.
- [23] G. Leclerc, G. Poullain, R. Bouregba, D. Chateigner, Influence of the substrate on ferroelectric properties of $\langle 111 \rangle$ oriented rhombohedral Pb(Zr_{0.6}Ti_{0.4})O₃ thin films, *Applied Surface Science.* 255 (2009) 4293–4297. <https://doi.org/10.1016/j.apsusc.2008.11.033>.
- [24] G. Velu, D. Remiens, Electrical properties of sputtered PZT films on stabilized platinum electrode, *Journal of the European Ceramic Society.* 19 (1999) 2005–2013.
- [25] B. Vilquin, G. Le Rhun, R. Bouregba, G. Poullain, H. Murray, Effect of in situ Pt bottom electrode deposition and of Pt top electrode preparation on PZT thin films properties, *Applied Surface Science.* 195 (2002) 63–73.
- [26] Y. Guo, D. Akai, K. Sawada, M. Ishida, The performance of Pt bottom electrode and PZT films deposited on Al₂O₃/Si substrate by using LaNiO₃ film as an adhesion layer, *Solid State Communications.* 145 (2008) 413–417.
- [27] J.P.B. Silva, K.C. Sekhar, A. Almeida, J.A. Moreira, J. Martín-Sánchez, M. Pereira, A. Khodorov, M.J.M. Gomes, Effect of Pt bottom electrode texture selection on the tetragonality and physical properties of Ba_{0.8}Sr_{0.2}TiO₃ thin films produced by pulsed laser deposition, *Journal of Applied Physics.* 112 (2012) 044105.
- [28] X. Zhu, E. Defay, M. Aïd, Y. Ren, C. Zhang, J. Zhu, J. Zhu, D. Xiao, Preferential growth and enhanced dielectric properties of Ba_{0.7}Sr_{0.3}TiO₃ thin films with preannealed Pt bottom electrode, *Journal of Physics D: Applied Physics.* 46 (2013) 105301.
- [29] T.K. Galeev, N.N. Bulgakov, G.A. Savelieva, N.M. Popova, Surface properties of platinum and palladium, *Reaction Kinetics and Catalysis Letters.* 14 (1980) 61–65.
- [30] C.C. Mardare, E. Joanni, A.I. Mardare, J.R.A. Fernandes, C.P.M. de Sá, P.B. Tavares, Effects of adhesion layer (Ti or Zr) and Pt deposition temperature on the properties of

- PZT thin films deposited by RF magnetron sputtering, *Applied Surface Science*. 243 (2005) 113–124. <https://doi.org/10.1016/j.apsusc.2004.09.050>.
- [31] R.M. Tiggelaar, R.G.P. Sanders, A.W. Groenland, J.G.E. Gardeniers, Stability of thin platinum films implemented in high-temperature microdevices, *Sensors and Actuators A: Physical*. 152 (2009) 39–47. <https://doi.org/10.1016/j.sna.2009.03.017>.
- [32] M.H. Kim, T.-S. Park, D.-S. Lee, E. Yoon, D.-Y. Park, H.-J. Woo, D.-I. Chun, J. Ha, Highly (200)-oriented Pt films on SiO₂/Si substrates by seed selection through amorphization and controlled grain growth, *Journal of Materials Research*. 14 (1999) 634–637. <https://doi.org/10.1557/JMR.1999.0641>.
- [33] D.-S. Lee, D.-Y. Park, H.-J. Woo, S.-H. Kim, J. Ha, E. Yoon, Preferred Orientation Controlled Giant Grain Growth of Platinum Thin Films on SiO₂/Si Substrates, *Jpn. J. Appl. Phys.* 40 (2001) L1–L3. <https://doi.org/10.1143/JJAP.40.L1>.
- [34] D.-Y. Park, D.-S. Lee, M.H. Kim, T.-S. Park, H.-J. Woo, E. Yoon, D. Chun, J. Ha, (100) Oriented Platinum thin Films Deposited by Dc Magnetron Sputtering On SiO₂/Si Substrates, *MRS Online Proceedings Library Archive*. 441 (1996). <https://doi.org/10.1557/PROC-441-335>.
- [35] D. Akai, K. Hirabayashi, M. Yokawa, K. Sawada, M. Ishida, Epitaxial growth of Pt(001) thin films on Si substrates using an epitaxial γ -Al₂O₃(001) buffer layer, *Journal of Crystal Growth*. 264 (2004) 463–467. <https://doi.org/10.1016/j.jcrysgro.2003.12.048>.
- [36] K. Kikuta, K. Noda, S. Okumura, T. Yamaguchi, S. Hirano, Orientation control of perovskite thin films on glass substrates by the application of a seed layer prepared from oxide nanosheets, *J Sol-Gel Sci Technol*. 42 (2007) 381–387.
- [37] T. Shibata, K. Fukuda, Y. Ebina, T. Kogure, T. Sasaki, One-Nanometer-Thick Seed Layer of Unilamellar Nanosheets Promotes Oriented Growth of Oxide Crystal Films, *Adv. Mater.* 20 (2008) 231–235.
- [38] T. Shibata, T. Ohnishi, I. Sakaguchi, M. Osada, K. Takada, T. Kogure, T. Sasaki, Well-controlled crystal growth of zinc oxide films on plastics at room temperature using 2D nanosheet seed layer, *The Journal of Physical Chemistry C*. 113 (2009) 19096–19101.
- [39] M. Bayraktar, A. Chopra, F. Bijkerk, G. Rijnders, Nanosheet controlled epitaxial growth of PbZr_{0.52}Ti_{0.48}O₃ thin films on glass substrates, *Applied Physics Letters*. 105 (2014) 132904.
- [40] T. Shibata, H. Takano, Y. Ebina, D.S. Kim, T.C. Ozawa, K. Akatsuka, T. Ohnishi, K. Takada, T. Kogure, T. Sasaki, Versatile van der Waals epitaxy-like growth of crystal films using two-dimensional nanosheets as a seed layer: orientation tuning of SrTiO₃

- films along three important axes on glass substrates, *Journal of Materials Chemistry C*. 2 (2014) 441–449.
- [41] M.D. Nguyen, E.P. Houwman, H. Yuan, B.J. Wylie-van Eerd, M. Dekkers, G. Koster, J.E. Ten Elshof, G. Rijnders, Controlling piezoelectric responses in $\text{Pb}(\text{Zr}_{0.52}\text{Ti}_{0.48})\text{O}_3$ films through deposition conditions and nanosheet buffer layers on glass, *ACS Applied Materials & Interfaces*. 9 (2017) 35947–35957.
- [42] A. Boileau, M. Dallochio, F. Baudouin, A. David, U. Lüders, B. Mercey, A. Pautrat, V. Demange, M. Guilloux-Viry, W. Prellier, Textured Manganite Films Anywhere, *ACS Applied Materials & Interfaces*. 11 (2019) 37302–37312.
- [43] V. Bouquet, F. Baudouin, V. Demange, S. Députier, S. Ollivier, L. Joanny, L. Rault, A. Fouchet, M. Guilloux-Viry, Influence of two-dimensional oxide nanosheets seed layers on the growth of (100) BiFeO_3 thin films synthesized by chemical solution deposition, *Thin Solid Films*. 693 (2020) 137687.
- [44] F. Baudouin, V. Demange, S. Ollivier, L. Rault, A.S. Brito, A.S. Maia, F. Gouttefangeas, V. Bouquet, S. Députier, B. Bérini, A. Fouchet, M. Guilloux-Viry, Orientation control of KNbO_3 film grown on glass substrates by $\text{Ca}_2\text{Nb}_3\text{O}_{10}$ nanosheets seed layer, *Thin Solid Films*. 693 (2020) 137682. <https://doi.org/10.1016/j.tsf.2019.137682>.
- [45] J.J. Manguelle, F. Baudouin, C. Cibert, B. Domengès, V. Demange, M. Guilloux-Viry, A. Fouchet, G. Poullain, Highly textured Pt thin film grown at very low temperature using $\text{Ca}_2\text{Nb}_3\text{O}_{10}$ nanosheets as seed layer, *SN Appl. Sci.* 2 (2020) 453. <https://doi.org/10.1007/s42452-020-2271-9>.
- [46] Y. Ebina, K. Akatsuka, K. Fukuda, T. Sasaki, Synthesis and in situ X-ray diffraction characterization of two-dimensional perovskite-type oxide colloids with a controlled molecular thickness, *Chemistry of Materials*. 24 (2012) 4201–4208.
- [47] D.K. Owens, R.C. Wendt, Estimation of the surface free energy of polymers, *Journal of Applied Polymer Science*. 13 (1969) 1741–1747.
- [48] B.-W. Li, M. Osada, Y. Ebina, K. Akatsuka, K. Fukuda, T. Sasaki, High thermal robustness of molecularly thin perovskite nanosheets and implications for superior dielectric properties, *ACS Nano*. 8 (2014) 5449–5461.
- [49] K.H. Ahn, S. Baik, S.S. Kim, Change of growth orientation in Pt films epitaxially grown on $\text{MgO}(001)$ substrates by sputtering, *Journal of Materials Research*. 17 (2002) 2334–2338.

- [50] X. Chen, T. Garrent, S.W. Liu, Y. Lin, Q.Y. Zhang, C. Dong, C.L. Chen, Scanning tunnelling microscopy studies of growth morphology in highly epitaxial c-axis oriented Pt thin film on (001)SrTiO₃, *Surface Science*. 542 (2003) L655–L661.
- [51] X.M. Xu, J. Liu, Z. Yuan, J. Weaver, C.L. Chen, Y.R. Li, H. Gao, N. Shi, Single crystalline highly epitaxial Pt thin films on (001)SrTiO₃, *Applied Physics Letters*. 92 (2008) 102102.
- [52] M. Hecq, A. Hecq, Oxygen induced preferred orientation of dc sputtered platinum, *Journal of Vacuum Science and Technology*. 18 (1981) 219–222.
- [53] P. Zaumseil, High-resolution characterization of the forbidden Si 200 and Si 222 reflections, *J Appl Cryst*. 48 (2015) 528–532. <https://doi.org/10.1107/S1600576715004732>.
- [54] T. Hyde, Final Analysis: Crystallite Size Analysis of Supported Platinum Catalysts by XRD, *Platinum Metals Review*. 52 (2008) 129–130.
- [55] J. Narayan, P. Tiwari, K. Jagannadham, O.W. Holland, Formation of epitaxial and textured platinum films on ceramics-(100)MgO single crystals by pulsed laser deposition, *Applied Physics Letters*. 64 (1994) 2093–2095.
- [56] M.H. Kim, T.-S. Park, E. Yoon, D.-S. Lee, D.-Y. Park, H.-J. Woo, D.-I. Chun, J. Ha, Changes in Preferred Orientation of Pt Thin Films Deposited by dc Magnetron Sputtering Using Ar/O₂ Gas Mixtures, *Journal of Materials Research*. 14 (1999) 1255–1260. <https://doi.org/10.1557/JMR.1999.0171>.
- [57] C.-Y. Chien, J.-Y. Yeh, Y.-C. Huang, M.-T. Lin, P.-L. Liu, Ab-Initio Study of (111) to (001) Texture Transformation in Ag Thin Films, *Materials Transactions*. 60 (2019) 437–440.
- [58] E.M. Zielinski, R.P. Vinci, J.C. Bravman, The influence of strain energy minimization on abnormal grain growth in copper thin films, *MRS Online Proceedings Library (OPL)*. 391 (1995).
- [59] C.V. Thompson, R. Carel, Stress and grain growth in thin films, *Journal of the Mechanics and Physics of Solids*. 44 (1996) 657–673.
- [60] C.V. Thompson, R. Carel, Grain growth and texture evolution in thin films, in: *Materials Science Forum*, Trans Tech Publ, 1996: pp. 83–98.
- [61] C. Körber, J. Suffner, A. Klein, Surface energy controlled preferential orientation of thin films, *Journal of Physics D: Applied Physics*. 43 (2010) 055301.

- [62] S. Mourya, J. Jaiswal, G. Malik, B. Kumar, R. Chandra, Structural and optical characteristics of in-situ sputtered highly oriented 15R-SiC thin films on different substrates, *Journal of Applied Physics*. 123 (2018) 023109.
- [63] P. Singh, D. Kaur, Influence of film thickness on texture and electrical and optical properties of room temperature deposited nanocrystalline V₂O₅ thin films, *Journal of Applied Physics*. 103 (2008) 043507.
- [64] H. Achahbar, F. Bernard, E. Courjon, T. Baron, S. Balandras, Growth of textured aluminum films on LiNbO₃ piezoelectric substrate with ultrathin tantalum underlayer., in: *2020 Symposium on Design, Test, Integration & Packaging of MEMS and MOEMS (DTIP)*, IEEE, 2020: pp. 1–5.
- [65] X.Y. Qiu, R.X. Wang, G.Q. Li, T. Zhang, L.T. Li, M.L. Wei, X.S. Meng, H. Ji, Z. Zhang, C.H. Chan, Oxygen-dependent epitaxial growth of Pt(001) thin films on MgO(001) by magnetron sputtering, *Applied Surface Science*. 406 (2017) 212–217.
- [66] M.H. Kim, T.-S. Park, D.-S. Lee, Y.E. Lee, D.-Y. Park, H.-J. Woo, D.-I. Chun, E. Yoon, J. Ha, Stress of Platinum Thin Films Deposited by Dc Magnetron Sputtering Using Argon/Oxygen Gas Mixture, *MRS Proc.* 441 (1996) 427. <https://doi.org/10.1557/PROC-441-427>.